energies

MDPI

Article

A Single-Phase Bidirectional AC/DC Converter for V2G Applications

Tao Peng [1], Peng Yang [1], Hanbing Dan [1,*], Hui Wang [1], Hua Han [1], Jian Yang [1], Hao Wang [1], Hui Dong [1] and Patrick Wheeler [2]

[1] School of Information Science and Engineering, Central South University, Changsha 410083, China; pandtao@csu.edu.cn (T.P.); yangpengwh@csu.edu.cn (P.Y.); wanghuicp9@csu.edu.cn (H.W.); hua_han0523@csu.edu.cn (H.H.); jian.yang@csu.edu.cn (J.Y.); wanghao930603@csu.edu.cn (H.W.); huyudong@csu.edu.cn (H.D.)

[2] Department of Electrical and Electronic Engineering, The University of Nottingham, Nottingham NG7 2RD, UK; pat.wheeler@nottingham.ac.uk

* Correspondence: daniel698@sina.cn; Tel.: +44-074-21-876780

Received: 18 May 2017; Accepted: 26 June 2017; Published: 30 June 2017

Abstract: This paper presents a single-phase bidirectional current-source AC/DC converter for vehicle to grid (V2G) applications. The presented converter consists of a line frequency commutated unfolding bridge and an interleaved buck-boost stage. The low semiconductor losses of the line frequency commutated unfolding bridge contribute to the comparatively good efficiency of this converter. The buck and boost operating modes of the interleaved buck-boost stage provide operation over a wide battery voltage range. The interleaved structure of the interleaved buck-boost stage results in lower battery current ripple. In addition, sinusoidal input current, bidirectional power flow and reactive power compensation capability are also guaranteed. This paper presents the topology and operating principles of the presented converter. The feasibility of the converter is validated using MATLAB simulations, as well as experimental results.

Keywords: bidirectional AC/DC converter; reactive power compensation capability; semiconductor losses; single-phase; V2G; wide battery voltage range

1. Introduction

Currently, as the representative of the renewable energy vehicles, plug-in hybrid electric vehicles (PHEV) and electrical vehicles (EV) are beginning to play a major role in coping with energy shortages and environment pollution problems. Furthermore, EVs and PHEVs are also regarded as energy storage units, which could feed stored energy back to the grid when required. Vehicle-to-grid (V2G) technology is being used as the reference term for the two-way interaction between the electric vehicle and the grid [1,2]. EVs and PHEVs can offer a large number of advantages in this application, such as peak power regulating, peak load shifting, and non-loaded standby [3,4].

As an essential part of a V2G system, the battery charger can be used for bidirectional power flow with a sinusoidal input current and adjustable power factor. To prolong the life of the batteries, the battery charger should have low ripple of the battery current. The battery charger connects the grid to the vehicle or other DC load. As with household charging, the customers and developers are pursuing high efficiency and reliability at low cost. For V2G applications, the features of a battery charger, such as high power density, reactive power compensation capability, and low ripple of battery current, have become the focus of research attention [5,6].

In the past many different AC/DC converter topologies have been used as interfaces for EVs. A single-phase interleaved AC/DC boost converter for plug-in hybrid electric vehicles (PHEV) was proposed in [7], and other topologies that achieve the same functionality have been presented in [8].

The converters presented in [7,8] could reduce the ripple of the battery current, but they could only boost the input voltage, and the battery charger requirement of a wide output voltage range cannot be satisfied. In [9,10] unidirectional buck–boost converters were introduced; they not only improve the output voltage range, but also have low input current total harmonic distortion (THD). However, all the converters presented above can only be used to charge the battery, they cannot feed energy back from the batteries to the grid.

In [11], the AC/DC matrix converter was suggested as the V2G interface. It can achieve bidirectional power flow. However, a large number of semiconductor switches operating at a high switching frequency are required, which means higher switching losses. In [12], the dual-buck full-bridge inverter was introduced, which reduces the filter's size and the ripple of the grid current, at the cost of two additional free-wheeling diodes and inductors. Others have investigated two-stage topologies, which are composed of an AC/DC converter and a DC/DC converter [13–17]. However, conversion efficiency and power density are the main concerns of these converters.

In [18,19] a dual active-bridge (DAB) converter is considered due to its simple topology and good output waveforms, but the current in the circulation process is high. In [20], a converter consisting of a single-phase current-source rectifier and an auxiliary switching network is proposed. It has high efficiency and offers bidirectional power flow. However, the circuit of the proposed topology is complex and the output current ripple is still large, which may reduce the battery life. Furthermore, all the converters mentioned above have no focus on reactive power compensation capability. To realize the reactive power operation, single-phase, on-board, bidirectional plug-in electric vehicle (PEV) chargers have been introduced [21]. The topology of the charger contains several characteristics such as simple structure, convenient control, and practicable construction. However, all the switches are operated at high frequency, which increases the power loss.

In order to simultaneously satisfy the function of bidirectional power flow, reactive power compensation capability and high efficiency, this paper presents a bidirectional current-source converter for V2G applications, which includes an AC/DC and a DC/DC conversion stage. Aiming to extend battery life and improve the overall efficiency, the front-end stage commutates at the line frequency. Owing to the line-commutated front stage circuit, the presented converter could provide an extended output reactive power range. The rear-end stage uses the interleaving buck-boost configuration to charge or discharge the batteries with different voltage ranges and low ripple in the battery current. Direct power control and pulse width modulation (PWM) are employed to meet the power demand of the grid. By means of the V2G bidirectional charger, the grid can be supported by EVs when the charger acts as a reactive power compensator. The presented converter in this paper has been described in [22], and more principle details and experimental results are added in this paper.

This paper is organized as follows: In Section 2, the topology and operating principles of the presented converter are introduced followed by the modeling process, modulation and control strategy. In Section 3, the semiconductor losses of the presented topology are analyzed. In Section 4, the simulation and experimental results are presented. The main points of this paper are summarized in Section 5.

2. Topology and Modeling

2.1. Topology of the Presented Converter

Figure 1 shows the topology of the presented current-source converter. The front-end stage consists of an inductance-capacitance (LC) input filter and a full-bridge converter, the rear-end stage consists of an interleaved parallel bidirectional buck-boost DC/DC converter and batteries.

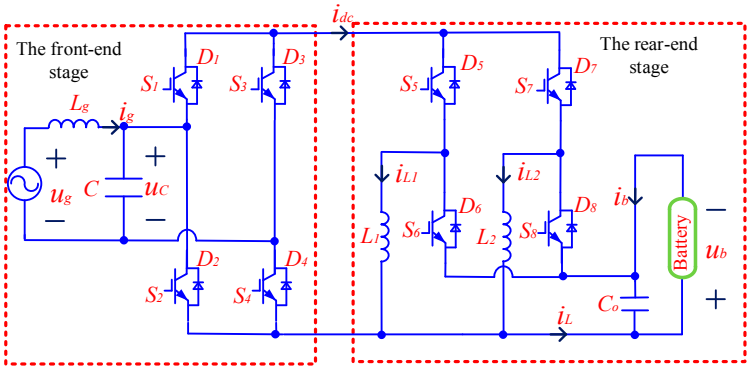

Figure 1. The presented bidirectional converter topology.

The LC input filter is used to prevent the high-frequency harmonic currents generated by the converter from flowing into grid. The full-bridge converter is used to rectify the AC input voltage to a DC voltage or invert the DC voltage to an AC voltage. Moreover, the bidirectional power flow is achieved. To improve the converter efficiency, the switches of the full-bridge converter commutate at the line frequency. The interleaved parallel bidirectional buck-boost DC/DC converter is employed to reduce the battery current ripple. Additionally, power factor correction (PFC) and high input current quality can be realized with the topology.

2.2. Operation Mode

Taking the charging state as an example, the operation of the presented converter topology is shown in Figure 2. Assume the duty-cycle d_1 is less than 0.5 and the grid voltage u_g is greater than zero, the operation mode is shown as follows.

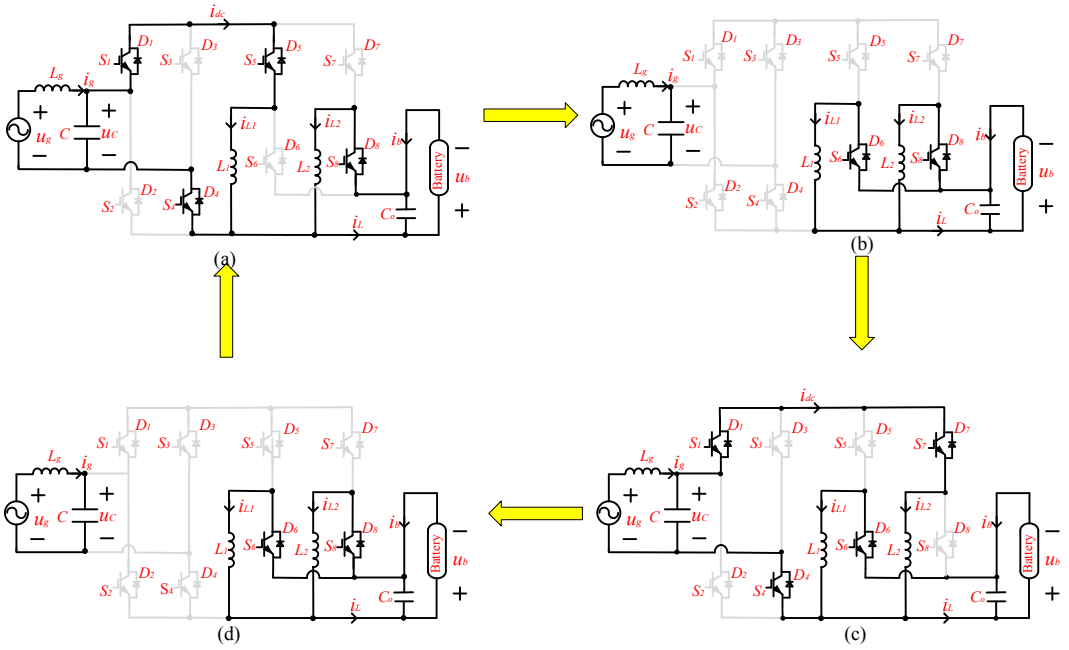

Figure 2. The operation mode of the interleaved parallel bidirectional buck-boost DC/DC circuit.

State 1 (t1–t2): from Figure 2a, S_5, S_8 are on, S_6, S_7 are off. The voltage across inductor L_1 is expressed as: $u_{L_1} = |u_g|$. u_{L_1} is positive, increasing linearly with a slope of $(|u_g|)/L$. And the energy is transferred from the grid to the inductor L_1. The voltage across inductor L_2 is expressed as: $u_{L_2} = -u_b$,

u_{L_2} is negative, i_{L_2} decreases linearly with a slope of $(u_b)/L$. The energy stored in the inductor L_2 is transferred to the battery.

State 2 (t2–t3): from Figure 2b, S_6, S_8 are on and S_5, S_7 are off. The energy in the inductors L_1, L_2 is transferred to the battery through S_6 and S_8. During this interval, the two inductor currents i_{L_1} and i_{L_2} decrease linearly with a slope of $(u_b)/L$.

State 3 (t3–t4): from Figure 2c, S_6, S_7 are on and S_5, S_8 are off. u_{L_2} is positive and the energy is transferred from the grid to the inductor L_2. u_{L_1} is negative and the energy stored in the inductor L_1 is transferred to the battery.

State 4 (t4–t5): from Figure 2d, S_6, S_8 are on and S_5, S_7 are off. This state is the same as state 2, so the energy in the inductors L_1, L_2 is transferred to the battery through S_6 and S_8.

In addition, the converter is able to work in other modes, and the similar analysis method can be applied. Therefore, due to space limits, the details are neglected here.

2.3. Modeling of the Presented Topology

According to Figure 1, assume that the system works in continuous conduction mode, the state space average model for the presented charger topology is formulated as follows:

$$\begin{cases} u_g = U_m \sin(\omega t) \\ i_g = I_m \sin(\omega t + \varphi) \\ Lg\frac{dig}{dt} = u_g - u_c \\ C\frac{duc}{dt} = ig - \mathrm{sgn}(u_C) d_1 i_L \\ i_{dc} = \mathrm{sgn}(u_g) i_g \\ i_L = i_{L_1} + i_{L_2} \\ L\frac{di_L}{dt} = d_1|u_C| - (1-d_1)u_b \end{cases} \tag{1}$$

where u_g is the grid voltage; i_g is the input current; U_m and I_m are the amplitude of the grid voltage and the input current, respectively. φ is the power factor angle. If $\varphi \in (-\pi/2, \pi/2)$, the grid will charge the batteries of the EV; if $\varphi \in (-\pi, -\pi/2) \cup (\pi/2, \pi)$, the batteries of the EV will be discharged. More importantly, active power and reactive power are absorbed from the grid or supported to the grid depending on power factor angle φ that is listed in Table 1. L_g and C are the inductance and capacitance of the input filter, respectively; u_C is the terminal voltage of capacitor C; i_{dc} is the current on DC side; u_b is the battery voltage; i_{L_1} and i_{L_2} are the two inductor currents; d_1 is the duty-cycle of switches S_5 and S_7; $(1 - d_1)$ is the duty-cycle of switches S_6 and S_8; sgn( ) is the sign function.

Table 1. The active and reactive power related to phase angle.

Phase Angle	Active Power (P)	Reactive Power (Q)
$\varphi \in (-\pi, -\pi/2)$	$P < 0$, discharging	$Q > 0$ Reactive power absorbing
$\varphi = -\pi/2$	$P = 0$	
$\varphi \in (-\pi/2, 0)$	$P > 0$, charging	
$\varphi = 0$	$P > 0$, charging	$Q = 0$
$\varphi \in (0, \pi/2)$	$P > 0$, charging	$Q < 0$ Reactive power supporting
$\varphi = \pi/2$	$P = 0$	
$\varphi \in (\pi/2, \pi)$	$P < 0$, discharging	
$\varphi = \pi$	$P < 0$, discharging	$Q = 0$

If the input filter is designed properly, the effect of the input filter can be neglected, then $u_g \approx u_c$. Based on voltage-second balance principle:

$$d_1|u_C| = (1-d_1)u_b \tag{2}$$

$$i_{dc} = d_1 i_L \tag{3}$$

According to Equation (2), d_1 can be obtained as follows:

$$d_1 = \frac{u_b}{|u_C| + u_b} \tag{4}$$

The sum of two inductor current i_L can be given by:

$$i_L = \frac{\mathrm{sgn}(u_c) i_g}{d_1} = \frac{\mathrm{sgn}(u_c) i_g (|u_C| + u_b)}{u_b} \tag{5}$$

In practical application, the current i_L can be controlled to guarantee i_g approach sine wave. It is easy to find that the input displacement angle of the presented converter ranges from $-\pi/2$ to $\pi/2$.

2.4. Modulation and Control Strategy

As a connection circuit between grid and EV, the objective of the presented converter is two-fold: charging or discharging the battery and alterable input power factor. The desired input power factor is obtained by designing the reference value of active power and reactive power: P_{ref} and Q_{ref}. In this section, a direct power control strategy and modulation of two stage converter are adopted to make the actual value of active power and reactive power track P_{ref} and Q_{ref}.

2.4.1. Direct Power Control Strategy

In order to realize the power tracking, a control block diagram of the presented bidirectional converter is shown in Figure 3. To improve reactive power compensation capability, a double-loop control of inverters is presented. The inner-loop is inductor current control and the outer-loop is designed by power control. As shown in Figure 3, P_{ref} and Q_{ref} are the active power and reactive power reference commands. The feedback signals for P and Q are measured by the grid voltage u_g and input current i_g. I_d, I_q are the amplitude of the active power current i_d and reactive power current i_q, respectively. The phase-locked loop (PLL) is adopted to achieve the phase angle of the grid voltage [23]. The input current i_g and power factor angle φ are followed by:

$$\begin{cases} I_d = I_m \cos\varphi \\ I_q = I_m \sin\varphi \\ P = \frac{1}{2} U_m I_d \\ Q = -\frac{1}{2} U_m I_q \end{cases} \tag{6}$$

$$ig = \sqrt{Id^2 + Iq^2}\sin(\omega t + \varphi) \tag{7}$$

$$\varphi = \arctan^{-1}\frac{Iq}{Id} \tag{8}$$

i_{Lref} is set as the inner-loop input reference, it is designed according to Equation (5). Substituting Equations (6)–(8) into Equation (5), the reference i_{Lref} can be expressed as:

$$i_{Lref} = \frac{\mathrm{sgn}(u_c)(|u_C| + u_b)\sqrt{Id^2 + Iq^2}\sin(\omega t + \varphi)}{u_b} \tag{9}$$

To regulate the current through the inductor, a control scheme is presented including the feed-forward control and the proportional integration (PI) feedback control. The feed-forward control directly compensates the effect of the grid power, which increases the dynamic response of the current control. The PI feedback controller improves system stability and anti-disturbance ability.

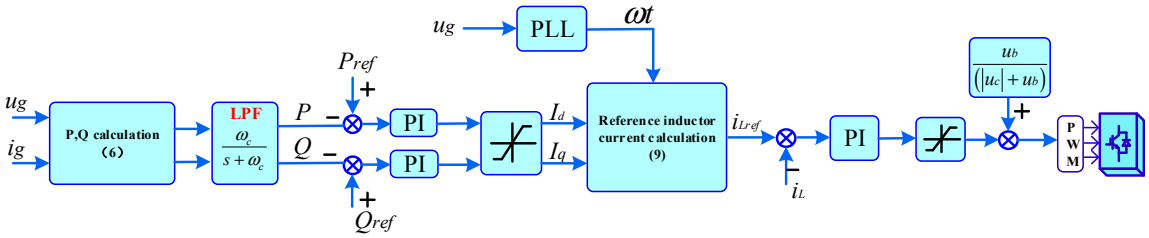

Figure 3. Control block diagram of the presented converter.

2.4.2. Modulation of the Two-Stage Converter

In the presented converter, the front-end stage AC/DC converter operates at the line frequency and the PWM modulation is adopted in the rear-end converter.

The front-end stage AC/DC converter operates at the line frequency, as shown in Figure 4. The power factor of the grid is alternative. S_{g1} is the switch level signal of S_1, S_4; S_{g2} is the switch level signal of S_2, S_3. When the grid voltage u_g is greater than zero, the switches S_1 and S_4 are turned on; switches S_2, S_3 are turned off. When u_g is less than zero, S_1 and S_4 are turned off, while S_2, S_3 are turned on.

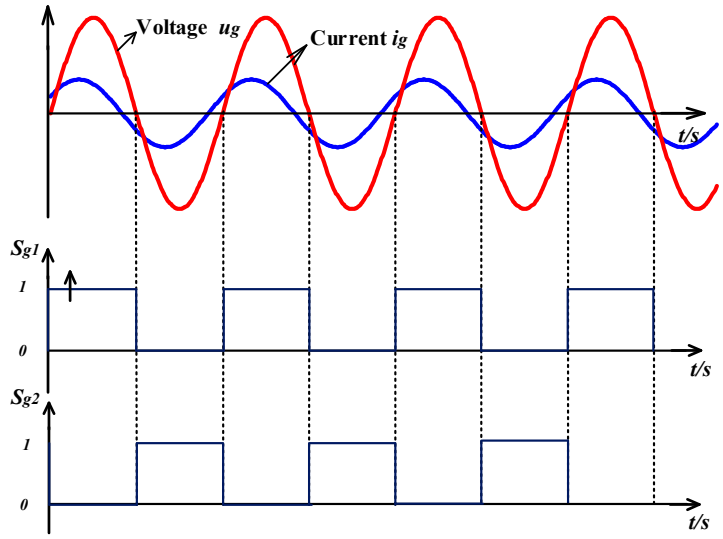

Figure 4. The front-end stage AC/DC converter operates at the line frequency.

The rear-end interleaved DC/DC converter adopts PWM modulation. From Figure 1, it has two identical inductors: $L_1 = L_2 = L$. Due to its configuration and modulation, it has low battery current ripple. As shown in Figure 5a,b, the shifted angle between the pulses of power switches S_3 and S_5 is π. Similarly, the pulses of power switches S_4 and S_6, mutually shifted, are the same. This modulation can reduce the battery current ripple to extend its life. To provide a bidirectional energy flow, the switches S_5, S_6 are in a complementary conduction state, as are the switches S_7 and S_8. The pulses of switches S_5, S_6, S_7, S_8, and the two inductor currents i_{L_1}, i_{L_2} are shown in Figure 5a. The total inductor current i_L ($i_L = i_{L_1} + i_{L_2}$) has little ripple.

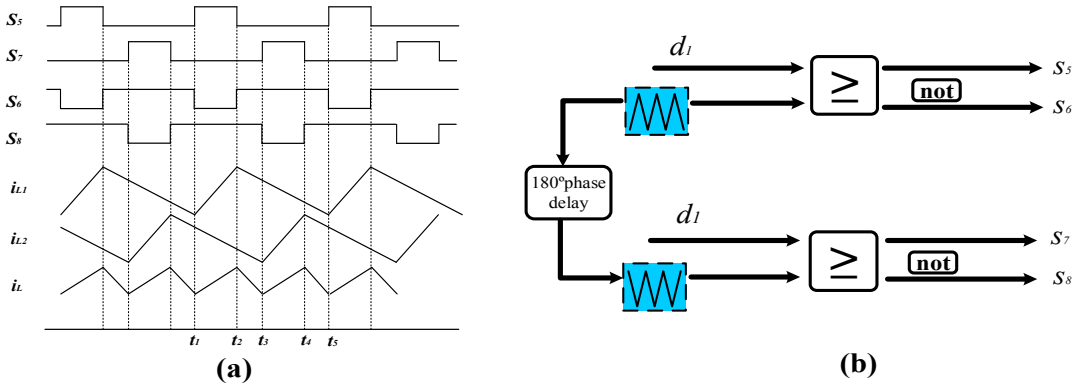

Figure 5. (**a**) The switch pulses and two inductor currents of the interleaved DC/DC converter; (**b**) The PWM modulation of the interleaved DC/DC converter.

3. Power Loss Analysis

To comprehend converter performance, calculation and analysis of the converter power loss are crucial, which influence the thermal design and predict the system efficiency. The power losses can be divided into two parts: semiconductor losses and passive components losses. In the presented converter, the semiconductor losses play the main role. Based on this, the power loss calculation of the semiconductors has become a top priority. In general, the semiconductor losses consist of conduction loss and switching loss, which shows a correlation with switching frequencies, current densities, and power requirements. In [24,25], the two main kinds of power semiconductor losses calculation formulas are as following.

Conduction loss:

$$P_{CS} = \frac{1}{T}\int_0^T \left(u_{CE0} i_c(t) + r_{CE} i_c^2(t)\right) dt \tag{10}$$

$$P_{CD} = \frac{1}{T}\int_0^T \left(u_{D0} \cdot i_D(t) + r_D \cdot i_D^2(t)\right) dt \tag{11}$$

where T is the period of the integrated function, P_{CS} and P_{CD} are the conduction loss of the insulated gate bipolar transistor (IGBT) and the conduction loss of the anti-parallel diode, respectively. u_{CE0} and u_{D0} are the forward voltages when the current is zero, they can be acquired by the incremental resistances of the IGBT r_{CE}, the diode r_D, and the flowing current i_c or i_D.

Switching loss:

$$P_{SWT} = \frac{f_s}{T}\int_0^T E_{SWT} \frac{v}{V_R} \frac{i}{I_R} dt \tag{12}$$

$$P_{SWD} = \frac{f_s}{T}\int_0^T E_{SWD} \frac{v}{V_R} \frac{i}{I_R} dt \tag{13}$$

where f_s is the switching frequency, P_{SWT} and P_{SWD} are the switching loss of the IGBT and the diode reverse recovery loss, respectively. E_{SWT} is the switching loss energy in the reference conditions (V_R and I_R), it includes the turn-on energy E_{on_T} and the turn-off energy E_{off_T} of the IGBT. E_{SWD} mainly includes the reverse recovery losses E_{rr_D}. Thus, it should be converted into the actual working conditions (v and i).

Based on the control and modulation scheme mentioned above, it's obvious that the presented converter has the same switching losses in charge or discharge mode and the conduction losses are different in these modes. Taking the charge mode, for example, in the front-end stage, the switches operate at line frequency, the conduction loss has become main part of the semiconductor loss and the switching loss has been neglected. The semiconductor loss in the rear-end interleaved parallel buck-boost converter consists of conduction loss and switching loss. Taking one arm S_5, S_6 for instance, in terms of switching loss, in the state 1 (S_5 is on and S_6 is off), the current i_L charge the inductor through

S_5. In the next state (state 2: S_5 is off and S_6 is on) the current i_L flows through the free-wheeling diode D_6. Then, in the last state (S_5 is on and S_6 is off), this state is similar to the state 1: S_5 turns on and S_6 is off, the current i_L charge the inductor through S_5 and the diode D_6 turn off. During this cyclical process, the turn-on and turn-off losses of S_5 and reverse recovery loss of D_6 are produced. Similarly, the conduction loss of the rear-end stage is mainly produced by the IGBT because of the neglected low conduction loss of body diode. In other modes, the analysis process for the other switches is similar.

From the front-end stage, the converter has two switches in the conducting state at any time. So the loss of the front-end stage can be expressed as:

$$P_{C\_front} = 2P_{CD} = \frac{2}{T}\int_0^T \left(u_{D0} \cdot i_D(t) + r_D \cdot i_D^2(t)\right) dt \tag{14}$$

From the rear-end stage, the converter has two parallel branches in DC/DC part. Assume that the root mean square (rms) of the total DC current is I_{dc}, each branch current is $I_{dc}/2$. The collector-emitter voltage rms of the switch is U_{SW}. The conduction loss P_{C_rear} and the switching loss P_{SW_rear} of the rear-end stage can be calculated by:

$$P_{C\_rear} = 2\left[(V_{D0} + V_{CE0})\frac{I_{dc}}{2} + (r_D + r_{CE})\left(\frac{I_{dc}}{2}\right)^2\right] \tag{15}$$

$$P_{SW\_rear} = 2\frac{f_s U_{SW}\frac{I_{dc}}{2}}{V_R I_R}\left(E_{on\_T} + E_{off\_T} + E_{rr\_D}\right) i_{L1} \tag{16}$$

The core losses P_{core} of DC inductor L_1 and L_2 can be calculated as:

$$P_{core} = 2K_{core}V_{core}(f_s)^m(B_{ac})^n \tag{17}$$

where K_{core} is the coefficient of the core material. V_{core} is the effective core volume. B_{ac} is the peak flux density. m and n is the frequency exponent and flux density exponent, respectively.

The wire losses P_{dcr} of DC inductor L_1 and L_2 caused by DC resistance can be calculated as:

$$P_{dcr} = 2I_{rms}^2 R_{dc} \tag{18}$$

where I_{rms} is the rms value of the peak current applied to the inductor, R_{dc} is the DC resistance of the inductor.

The total losses P_L of DC inductor L_1 and L_2 can be calculated as:

$$P_L = P_{core} + P_{dcr} \tag{19}$$

Finally, in the unity charging mode, the total loss of this AC/DC converter P_{total} can be acquired by equations:

$$P_{total} = P_{C\_front} + P_{C\_rear} + P_{SW\_rear} + P_L \tag{20}$$

The efficiency is estimated according to Equation (14)–(20), the results are shown in Figure 6. The efficiency changes as a function of the input current rms when the grid voltage is 220 V and the battery voltage is 120 V. It can be seen that the maximum efficiency is larger than 95%. When the input current rms is 2 A, after calculation and analysis, the efficiency of the converter is 94.79%. It is clear that when the input current rms is relatively small, the efficiency increases with the input power rms. Conversely, it decreases when the input current rms is larger. When the rms of the input current is 3 A, the power loss of each component has been listed in Table 2.

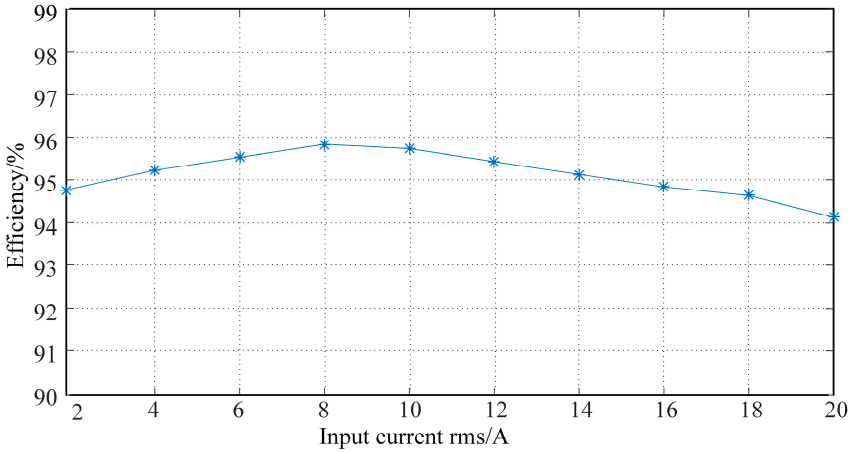

Figure 6. Efficiency variation with the input current rms.

Table 2. The power loss of each component when the rms of input current is 3 A.

Power Loss	Values
Front-end stage conduction loss of diodes $P_{c\_d\_front}$	8.94 W
Rear-end stage switching loss of IGBT $P_{sw\_T\_rear}$	6.73 W
Rear-end stage reverse-recovery loss of diodes $P_{sw\_d\_rear}$	7.30 W
Rear-end stage conduction loss of diodes $P_{c\_d\_rear}$	3.68 W
Rear-end stage conduction loss of IGBT $P_{c\_T\_rear}$	3.89 W
The losses of DC inductors P_L	3.06 W

4. Simulation and Experimental Results

4.1. Simulation Results

To validate the V2G bidirectional converter topology, simulations are implemented based on the MATLAB/Simulink environment in this section. The models of the semiconductor device and battery are from the SimPowerSystem/Power Electronics library. The schematic diagram of the presented bidirectional converter in the simulation is shown in Figure 1. The parameters used in the simulation are listed in Table 3. A switching frequency of 20 kHz is selected with the trade-off between THD and the converter efficiency. An input filter is used to avoid overvoltage and reduce input current distortion. The DC inductors L_1 and L_2 are working in the linear area of flux density-magnetic field strength (B-H) curve. The loads are 38 Ah-capacity lead-acid batteries with a nominal voltage of 120 V.

Table 3. Simulation parameters.

Parameters	Values
The amplitude of voltage U_g	311 V
Input filter inductance (L_g)	0.8 mH
Input filter capacitor (C)	10 uF
DC inductor L_1	0.2 mH
DC inductor L_2	0.2 mH
Output filter capacitor (C_o)	10^3 uF
Switching frequency (f_s)	20 kHz
Battery voltage (u_b)	120 V

The simulation results shown in Figure 7 show the performance of the presented converter. From the top to bottom, the grid voltage u_g, the input current i_g; the inductor L_1 current i_{L_1}; the duty-cycle of switch S_5; the battery voltage u_b and the battery current i_b are sequentially displayed. The simulation

results in four different modes are shown in Figure 7. The simulation starts with the charging operation and is changed to the discharging operation at 0.05 s.

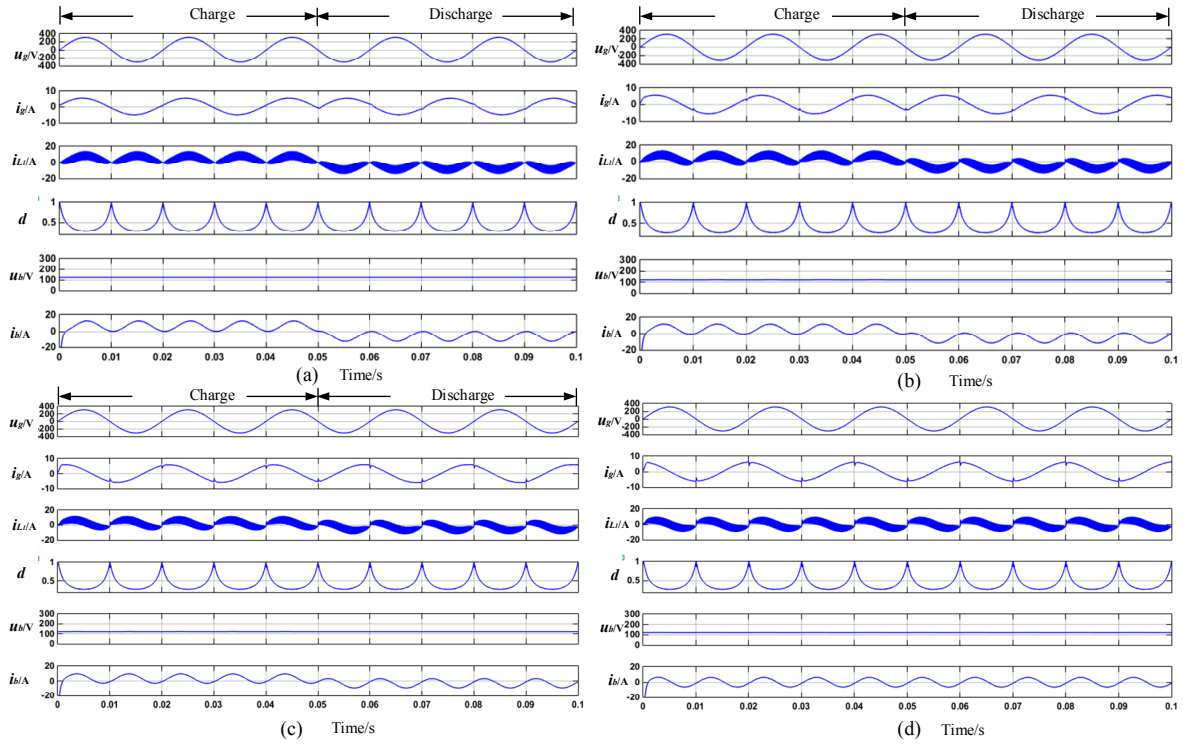

Figure 7. The presented converter charge or discharge at different power factors: (**a**) Unity power factor; (**b**) power factor: $cos\varphi = \pm\sqrt{3}/2$; (**c**) power factor: $cos\varphi = \pm 0.5$; (**d**) power factor: $cos\varphi = 0$

As shown in Figure 7a, the presented V2G bidirectional charger works in the charging or discharging mode under a unity power factor ($cos\varphi = \pm 1$). The THD of the input current is less than 3%. In Figure 7b, the power factor is $\pm\sqrt{3}/2$. No matter which mode (charging or discharging) the presented bidirectional converter operates in, they can supply the reactive power to the grid.

If the grid demand for reactive power is large, for example, when the power factor is ± 0.5, more reactive power would be supplied by the bidirectional chargers. The simulation is shown in Figure 7c, and the THD in the input current is less than 4%. When the EVs are not in the charging or discharging mode, they are only used as reactive power compensators (the power factor is 0) by the charges. The simulation is shown in Figure 7d, The THD of the input current is less than 5%. Seen from the simulation results in Figure 7, the ripple of the battery current is quite small.

However, it can be found that the inductor current is distorted near the grid voltage zero-crossing region in all of the charging modes, because the forward voltage drops of the IGBT and diodes make the inductor current lose control when the input voltage is small.

4.2. Experimental Results

A prototype for the presented converter has been developed in the laboratory to show the experimental verification. As shown in Figure 8, the experimental prototype has two main units: (1) the main power board; (2) the control board. The main power board has the main AC/DC circuit and several gate drive circuits. The IGBTs used in the main circuit are IKW30N60DTP (Infineon, Milpitas, CA, USA). The core material of the DC inductor is "Kool Mμ-77192A7" (Magnetics, Pittsburgh, PA, USA). A floating point Texas Instruments digital signal processor (DSP, TMS320F28335, Texas Instruments, Dallas, TX, USA) is used to calculate the duty ratios of the switches in the presented V2G bidirectional converter topology. Meanwhile, a field programmable

gate array (FPGA, EP2C8T144C8N, Altera Corporation, San Jose, CA, USA) is used for implementing the operation mode of the switches.

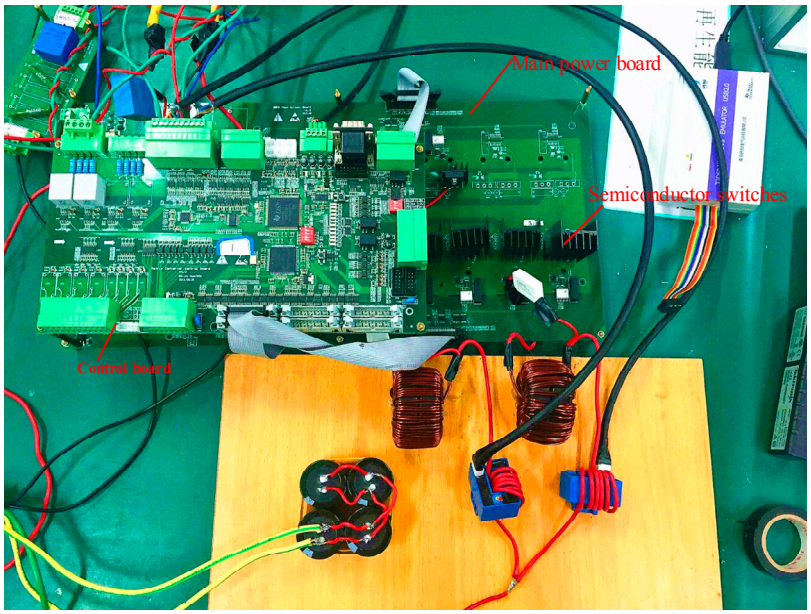

Figure 8. A prototype for the presented converter.

The experimental results presented in Figures 9–11 show the operation of the presented single-phase bidirectional converter with the battery voltage 120 V/38 Ah and the grid voltage in the charging mode. In Figure 12, the presented converter operates under unity power factor in the discharging mode. The experimental results of the grid voltage, input current, inductor current, and battery voltage under different conditions are presented in Figures 9–12. The THD values of the input current in Figures 9–12 have been presented in Table 4, respectively.

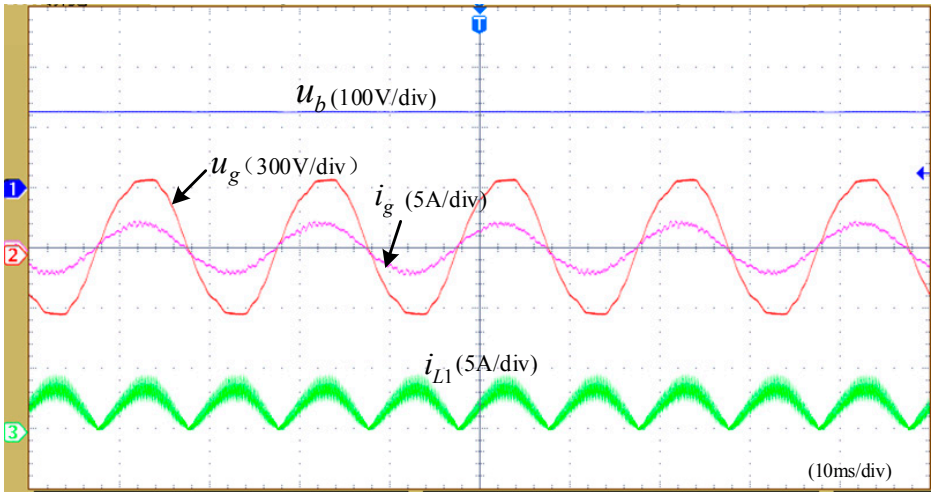

Figure 9. The experimental waveform of the presented converter operating in charging mode under a unity power factor (P = 400 W, Q = 0 var, $cos\varphi = 1$.

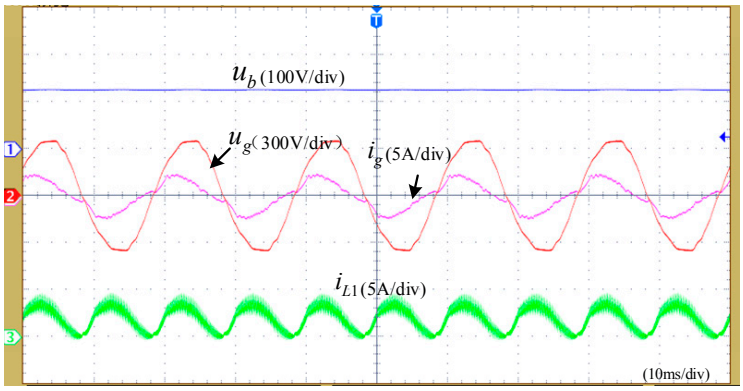

Figure 10. The experimental waveform of the presented converter operating in the charging mode (P = 200 W, Q = −340 var, $cos\varphi$ = 0.5.

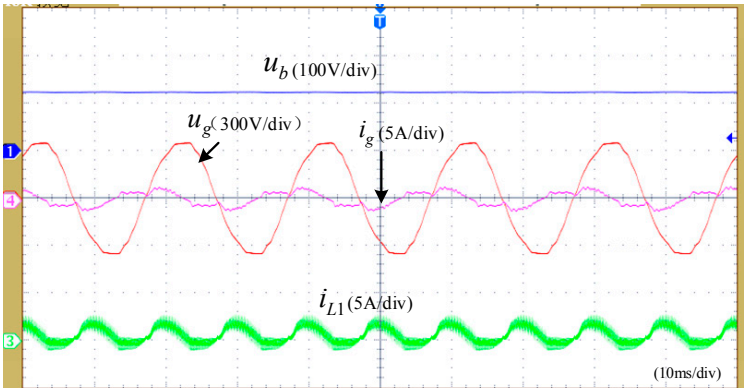

Figure 11. The experimental waveform of the presented converter operating as reactive power compensation equipment (P = 0, Q = −400 var, $cos\varphi$ = 0.

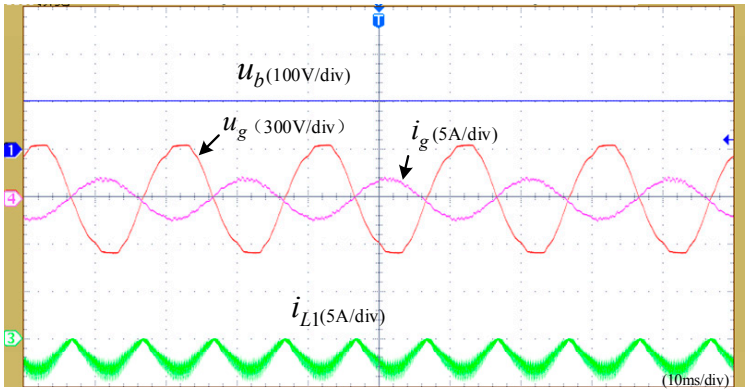

Figure 12. The experimental waveform of the presented converter operating in the discharging mode under a unity power factor (P = −400 W, Q = 0 var, $cos\varphi$ = −1.

Table 4. The THD values of input current under different conditions.

Condition	The THD of Input Current
P = 400 W, Q = 0 var, $cos\varphi$ = 1	6.15%
P = 200 W, Q = −340 var, $cos\varphi$ = 0.5	18.33%
P = 0, Q = −400 var, $cos\varphi$ = 0	34.58%
P = −400 W, Q = 0 var, $cos\varphi$ = −1	7.31%

In the charging mode, the presented converter operated under a unity power factor, as shown in Figure 9. The active power P is 400 W, and the THD value of the input current is nearly sinusoidal. In other conditions, as shown in Figure 10, the power factor is 0.5, the active power P is 200 W, and the reactive power Q is -340 var. The THD value of the input current is worse than the condition under a unity power factor. Obviously, the converter has supported a part of reactive power. Especially, the presented converter can be operated as reactive power equipment compensation as presented in Figure 11. It does not transmit active power in this condition. The power factor angle is $\pi/2$ and the reactive power is -400 var. However, it can be found that the inductor current is distorted near the grid voltage zero-crossing region in non-unity power factor modes, which leads to distortion of the input current. This is because the forward voltage drops of the IGBT and diode make the inductor current lose control when the input voltage is small. To feed energy back to the grid, the converter should operate in the discharging mode. As shown in Figure 12, the converter operates under a unity power factor in the discharging mode, and the active power is -400 W. It can be seen that the power factor angle between input current and grid voltage is almost π. In addition, the input current is nearly sinusoidal. Due to the converter's interleaved configuration and modulation, it can be seen that the total inductor current ripple has been reduced in Figures 13 and 14. All the experimental results mentioned above show that the presented converter is suitable to take an indispensable role for V2G applications.

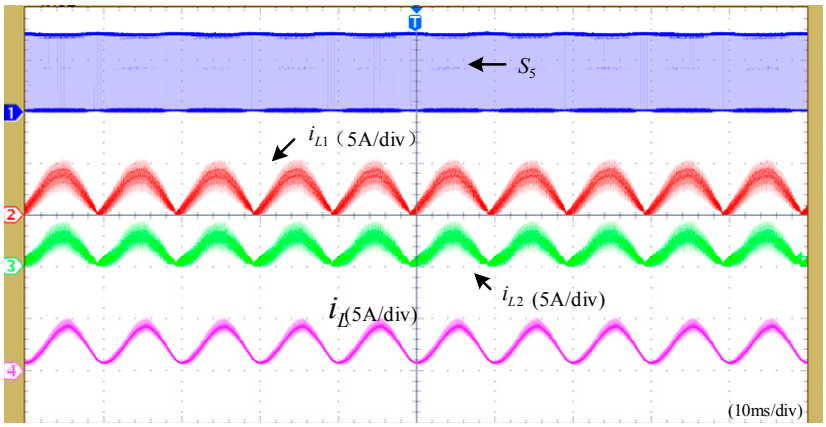

Figure 13. The experimental waveform of the inductor currents operating in the charging mode under a unity power factor (P = 400 W, Q = 0 var, $cos\varphi = 1$.

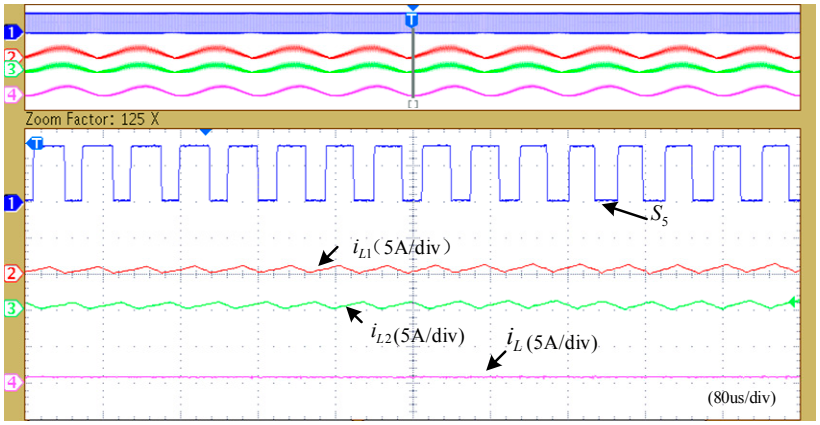

Figure 14. The enlarged drawing of Figure 13.

5. Conclusions

In this paper a single-phase bidirectional AC/DC converter for V2G applications has been presented. This topology consists of a line frequency-commutated unfolding bridge and an interleaved buck-boost stage. The circuit operates in buck-boost charging/discharging condition, and offers different voltage levels for all types of batteries. The operation principle of the presented charger topology has been analyzed and it has been shown that reactive power can be supported and exchanged with the grid using the presented bidirectional charger. Moreover, the presented charger has a number of attractive features, such as bidirectional power flow, low current ripple, and a wide battery voltage range. Thus, it is a good candidate for V2G applications. The simulation and experimental results have been presented to verify the effectiveness of the V2G bidirectional charger.

Acknowledgments: This work was supported by the Major Program of the National Natural Science Foundation of China under grants 61490702 and 61573384, and the Fundamental Research Funds for the Central Universities of Central South University under Grant 2017zzts687.

Author Contributions: Peng Yang conceived the main idea and wrote the manuscript with guidance from Tao Peng and Hui Wang. Hao Wang and Hui Dong performed the experiments; Hanbing Dan, Hua Han, Jian Yang and Patrick wheeler reviewed the work and gave helpful improvement suggestions.

Conflicts of Interest: The authors declare no conflict of interest.

References

1. Kempton, W.; Tomic, J. Vehicle-to-grid power fundamentals: Calculating capacity and net revenue. *J. Power Sources* **2005**, *144*, 268–279. [CrossRef]
2. Viswanathan, V.V.; Kintner-Meyer, M. Second use of transportation batteries: Maximizing the value of batteries for transportation and grid services. *IEEE Trans. Veh. Technol.* **2011**, *60*, 2963–2970. [CrossRef]
3. Sortomme, E.; El-Sharkawi, M.A. Optimal scheduling of vehicle-to-grid energy and ancillary services. *IEEE Trans. Smart Grid* **2012**, *3*, 351–359. [CrossRef]
4. Yilmaz, M.; Krein, P.T. Review of the impact of vehicle-to-grid technologies on distribution systems and utility interfaces. *IEEE Trans. Power Electron.* **2013**, *28*, 5673–5689. [CrossRef]
5. Kisacikoglu, M.C.; Ozpineci, B.; Tolbert, L.M. EV/PHEV bidirectional charger assessment for V2G reactive power operation. *IEEE Trans. Power Electron.* **2013**, *28*, 5717–5727. [CrossRef]
6. Jang, M.; Ciobotaru, M.; Agelidis, V.G. A compact single-phase bidirectional buck-boost inverter topology. In Proceedings of the 2012 International Conference on Renewable Energy Research and Applications (ICRERA), Nagasaki, Japan, 11–14 November 2012; pp. 1–6.
7. Jang, Y.; Jovanovic, M.M. Interleaved boost converter with intrinsic voltage-doubler characteristic for universal-line PFC front end. *IEEE Trans. Power Electron.* **2007**, *22*, 1394–1401. [CrossRef]
8. Musavi, F.; Eberle, W.; Dunford, W.G. A high-performance single-phase bridgeless interleaved PFC converter for plug-in hybrid electric vehicle battery chargers. *IEEE Trans. Ind. Appl.* **2011**, *47*, 1833–1843. [CrossRef]
9. Lopez, O.; De Vicuna, L.C.; Castilla, M.; Matas, J.; Lopez, M. Sliding-mode-control design of a high-power-factor buck-boost rectifier. *IEEE Trans. Ind. Electron.* **1999**, *46*, 604–612. [CrossRef]
10. Ghanem, M.C.; Al-Haddad, K.; Roy, G. A new control strategy to achieve sinusoidal line current in a cascade buck-boost converter. *IEEE Trans. Ind. Electron.* **1996**, *43*, 441–449. [CrossRef]
11. Su, M.; Wang, H.; Sun, Y.; Yang, J.; Xiong, W.; Liu, Y. AC/DC matrix converter with an optimized modulation strategy for V2G applications. *IEEE Trans. Power Electron.* **2013**, *28*, 5736–5745. [CrossRef]
12. Li, B.; Huang, S.; Chen, X. Performance improvement for two-stage single-phase grid-connected converters using a fast dc bus control scheme and a novel synchronous frame current controller. *Energies* **2017**, *10*, 389. [CrossRef]
13. Ngo, T.; Lee, K.; Won, J.; Nam, K. Study of single-phase bidirectional battery charger for high power application. In Proceedings of the 7th International Power Electronics and Motion Control Conference (IPEMC), Harbin, China, 2–5 June 2012; pp. 958–962.
14. Wong, N.; Kazerani, M. A review of bidirectional on-board charger topologies for plugin vehicles. In Proceedings of the 25th IEEE Canadian Conference on Electrical & Computer Engineering (CCECE), Montreal, QC, Canada, 29 April–2 May 2012; pp. 1–6.

15. Shin, J.; Lee, J.Y. An electrolytic capacitor-less bi-directional EV on-board charger using harmonic modulation technique. *IEEE Trans. Power Electron.* **2014**, *29*, 5195–5203. [CrossRef]
16. Yilmaz, M.; Krein, P.T. Review of battery charger topologies, charging power levels, and infrastructure for plug-in electric and hybrid vehicles. *IEEE Trans. Power Electron.* **2013**, *28*, 2151–2169. [CrossRef]
17. Choi, J.; Byen, B.; Lee, Y.; Han, D.; Kho, H.; Choe, G. Design of leakage inductance in resonant dc-dc converter for electric vehicle charger. *IEEE Trans. Magn.* **2012**, *48*, 4417–4420. [CrossRef]
18. Rosekeit, M.; Broeck, C.; De Doncker, R.W. Dynamic control of a dual active bridge for bidirectional ac charging. In Proceedings of the IEEE International Conference on Industrial Technology (ICIT), Seville, Spain, 17–19 March 2015; pp. 2085–2091.
19. Xue, L.; Shen, Z.; Boroyevich, D.; Mattavelli, P.; Diaz, D. Dual active bridge-based battery charger for plug-in hybrid electric vehicle with charging current containing low frequency ripple. *IEEE Trans. Power Electron.* **2015**, *30*, 7299–7307. [CrossRef]
20. Han, H.; Liu, Y.; Sun, Y.; Wang, H.; Su, M. A single-phase current-source bidirectional converter for V2G applications. *J. Power Electron.* **2014**, *14*, 458–467. [CrossRef]
21. Kisacikoglu, M.C.; Kesler, M. Single-phase on-board bidirectional PEV charger for V2G reactive power operation. *IEEE Trans. Smart Grid* **2015**, *6*, 767–775. [CrossRef]
22. Yang, P.; Peng, T.; Wang, H.; Han, H.; Yang, J.; Wang, H. A single-phase current-source bidirectional converter for V2G application. In Proceedings of the IEEE 3rd International Future Energy Electronics Conference 2017 and ECCE Asia (IFEEC 2017-ECCEAsia), Kaohsiung, Taiwan, 3–7 June 2017.
23. Luo, Z.; Su, M.; Sun, Y.; Liu, Z.; Dong, M. First-order generalized integrator based frequency-locked loop and synchronization for three-phase grid-connected converters under adverse grid conditions. *J. Power Electron.* **2016**, *16*, 1939–1949. [CrossRef]
24. Bierhoff, M.H.; Fuchs, F.W. Semiconductor losses in voltage source and current source IGBT converters based on analytical derivation. In Proceedings of the IEEE 35th Annual Power Electronics Specialists Conference, Aachen, Germany, 20–25 June 2004; pp. 2836–2842.
25. Wang, B.; Venkataramanan, G. Analytical modeling of semiconductor losses in matrix converters. In Proceedings of the 5th International Power Electronics and Motion Control Conference, Shanghai, China, 14–16 August 2006; pp. 1–8.